



PERGAMON

Available online at [www.sciencedirect.com](http://www.sciencedirect.com)

SCIENCE @ DIRECT®

International Journal of Hydrogen Energy 29 (2004) 465–473

International Journal of  
**HYDROGEN  
ENERGY**

[www.elsevier.com/locate/ijhydene](http://www.elsevier.com/locate/ijhydene)

# Density functional study of the adsorption and separation of hydrogen in single-walled carbon nanotube

Chong Gu, Guang-Hua Gao\*, Yang-Xin Yu

*Department of Chemical Engineering, Tsinghua University, Beijing 100084, People's Republic of China*

Received 18 January 2003; received in revised form 3 April 2003; accepted 3 April 2003

## Abstract

In this work, we report an investigation by means of density functional theory (DFT) of the adsorption of hydrogen and the separation of hydrogen–carbon monoxide mixture in an isolated single-walled carbon nanotube. The theory is based on a perturbative construction of free energy functional for inhomogeneous pure fluid and binary fluid mixture. The reformulated Rosenfeld's fundamental-measure theory using the excess Helmholtz energy density from the Boublik–Mansoori–Carnahan–Starling–Leland equation of state proposed by Yu and Wu (J. Chem. Phys. 117 (2002) 10156) is applied to represent the pure and binary hard-sphere repulsive interaction, and Weeks–Chandler–Andersen perturbation theory is used to build the attractive contribution. The density profiles in three sizes of tubes at 300 K and reduced bulk density from 0.2 to 0.7 for pure hydrogen and hydrogen–carbon monoxide mixture are obtained. The theoretical calculations are in good agreement with the simulation results in this work and other data available in literature. The adsorption of hydrogen and the selectivity of hydrogen–carbon monoxide mixture are predicted from DFT and the adsorption characteristics of the isolated cylindrical wall is discussed.

© 2003 International Association for Hydrogen Energy. Published by Elsevier Ltd. All rights reserved.

*Keywords:* Density functional theory; Hydrogen; Separation; Computer simulation

## 1. Introduction

In the past 10 years, carbon nanotube is being widely used in various areas. However, its applicability as an adsorbent of hydrogen for use in electric automobile is still being evaluated. Tremendous efforts have been made in the study of hydrogen adsorption in carbon nanotubes, including experiments [1,2], computer simulation [3–9], density functional theory (DFT) [10] and ab initio calculation [11]. Because of its powerful adsorption ability, the application of carbon nanotubes as a separation agent for mixtures is another interesting topic. Also some work has been done for this [12–21].

With proper models of interactive potential, Monte Carlo and molecular dynamics simulation provide good

descriptions of the adsorption, but the size of the system is always greatly limited by the computational cost. At this point, the DFT appears to be powerful tool. DFT of fluids near a wall has various forms: The local-density approximation (LDA) of Sullivan [22], the smoothed-density approach (SDA) due to Tarazona [23–25], the weighted-density approximation (WDA) due to Curtin and Ashcroft [26], the generalized van der Waals theory (GvdW) introduced by Freasier et al. [27] and the fundamental measure theory (FMT) proposed by Rosenfeld [28–31]. Among them, FMT is evaluated to be the most successful theory for prediction of strongly inhomogeneous hard spheres [32]. It has been successfully applied to describe the properties of hard spheres in the bulk and in slitlike pores, and also has been extended to molecular fluids [31–36]. Moreover, by using the same formulation for one-component fluids, the extension of FMT to multi-component systems is straightforward. However, the expression of excess free energy density in FMT originates from PY equation or the scaled particle theory, which usually gives bad estimation of contact

\* Corresponding author. Tel.: +86-10-6278-2558; fax: +86-10-6277-0304.

E-mail address: [gaogh@tsinghua.edu.cn](mailto:gaogh@tsinghua.edu.cn) (G.-H. Gao).

densities for nonuniform hard sphere fluids. Most recently, Yu and Wu [32] proposed a variation of the FMT. In their theory, the excess free energy density was based on the Boublik–Mansoori–Carnahan–Starling–Leland (BMCSL) equation of state, which was proved to give a better prediction of the contact value than PY equation.

In this study, we applied the modified FMT of Yu and Wu [32] to describe the hard-sphere contribution to hydrogen fluid and hydrogen–carbon monoxide mixture. And the WCA perturbation scheme is added to represent the attractive interaction. The inhomogeneity of the fluids in this system is caused by an external field of cylindrical pore. The theoretical results are compared with GCMC simulation data both in this work and in literature. DFT is also used to calculate the adsorption and separation isotherms inside an isolated single-walled carbon nanotube.

## 2. Models and theory

Given temperature and chemical potential, the equilibrium behavior of the system can be represented by the system grand potential, which is expressed as

$$\Omega = F + \sum_{i=1}^K \int d\mathbf{r} \rho_i(\mathbf{r})(\psi(\mathbf{r}) - \mu_i), \quad (1)$$

where  $\rho_i(\mathbf{r})$  and  $\mu_i$  are the number density and the chemical potential of bulk species  $i$ , respectively.  $\Omega$  and  $F$  are the grand potential functional and the intrinsic Helmholtz free energy functional. On the left side of Eq. (1),  $K = 1$  is for pure fluid and  $K = 2$  for binary mixtures.  $\psi(\mathbf{r})$  represents the external potential. The integrals are carried out over the system volume. The equilibrium density distribution satisfies the stationary condition

$$\frac{\delta\Omega}{\delta\rho_i(\mathbf{r})} = 0, \quad (2)$$

where  $\rho_i(\mathbf{r})$  is the equilibrium density. The Helmholtz free energy described in our model can be split into two parts,  $F = F_{\text{id}} + F_{\text{ex}}$ .  $F_{\text{id}}$  is the ideal gas contribution, and its expression is known exactly.

$$\beta F_{\text{id}} = \sum_{i=1}^K \int d\mathbf{r} \rho_i(\mathbf{r}) \{ \ln[\rho_i(\mathbf{r})] - 1 \}, \quad (3)$$

where  $\beta = 1/kT$  and  $k$  is the Boltzmann constant.

In Rosenfeld's FMT, the excess Helmholtz free energy functional of an inhomogeneous hard-sphere mixture can be expressed in the form of a WDA. And to represent the hydrogen molecule, an item of soft attraction  $\beta F_{\text{att}}$  is added, therefore,

$$\beta F_{\text{ex}} = \int \phi(\mathbf{r}) d\mathbf{r} + \beta F_{\text{att}}, \quad (4)$$

where, the reduced excess Helmholtz energy density  $\phi$  is a function of the weighted averages of the density distribution functions  $\rho_i(\mathbf{r})$ .

The weighted density can be expressed as

$$n_\alpha(\mathbf{r}) = \sum_i n_{\alpha,i}(\mathbf{r}) = \sum_i \int \rho(\mathbf{r}') w_i^{(\alpha)}(\mathbf{r} - \mathbf{r}') d\mathbf{r}', \quad (5)$$

where the subscripts  $\alpha = 0, 1, 2, 3, V1, V2$  denote the index of six weight functions  $w^{(\alpha)}(r)$ , i.e.,

$$w_i^{(2)}(\mathbf{r}) = \delta(d_i/2 - r), \quad (6)$$

$$w_i^{(3)}(\mathbf{r}) = \Theta(d_i/2 - r), \quad (7)$$

$$\mathbf{w}_i^{(V2)}(\mathbf{r}) = (\mathbf{r}/r)\delta(d_i/2 - r), \quad (8)$$

where  $\delta(r)$  denotes the Dirac delta function and  $\Theta(r)$  is the Heaviside step function. Integration of the two scalar functions,  $w_i^{(2)}(\mathbf{r})$  and  $w_i^{(3)}(\mathbf{r})$ , with respect to position gives, respectively, the particle surface area and volume; and integration of the vector function  $\mathbf{w}_i^{(V2)}(\mathbf{r})$  is related to the gradient across a sphere in the  $\mathbf{r}$  direction. Therefore, these three functions are directly related to the geometry of a spherical particle. The other three are proportional to them,

$$\begin{aligned} w_i^{(0)}(\mathbf{r}) &= \frac{w_i^{(2)}(\mathbf{r})}{\pi d_i^2}, \\ w_i^{(1)}(\mathbf{r}) &= \frac{w_i^{(2)}(\mathbf{r})}{2\pi d_i}, \\ \mathbf{w}_i^{(V1)}(\mathbf{r}) &= \frac{\mathbf{w}_i^{(V2)}(\mathbf{r})}{2\pi d_i}, \end{aligned} \quad (9)$$

where  $d_i$  represents the diameter of a hard sphere.

Consequently, the reformulated excess free energy density consists of a scalar and a vector contributions

$$\phi = \phi^S + \phi^V, \quad (10)$$

The expressions of  $\phi^S$  and  $\phi^V$  are derived by Yu and Wu [32],

$$\begin{aligned} \phi^S &= -n_0 \ln(1 - n_3) + \frac{n_1 n_2}{1 - n_3} \\ &+ \left[ \frac{1}{36\pi n_3^2} \ln(1 - n_3) + \frac{1}{36\pi n_3(1 - n_3)^2} \right] n_2^3, \end{aligned} \quad (11)$$

which is the exact BMCSL equation of state for bulk hard sphere fluid, and the vector weighted density contribution directly results from the comparison of the dimensionalities between the coefficients of the scalar and vector weighted densities in Rosenfeld's former expression [37]

$$\begin{aligned} \phi^V &= -\frac{\mathbf{n}_{V1} \cdot \mathbf{n}_{V2}}{1 - n_3} - \left[ \frac{1}{12\pi n_3^2} \ln(1 - n_3) \right. \\ &\left. + \frac{1}{12\pi n_3(1 - n_3)^2} \right] n_2 \mathbf{n}_{V1} \cdot \mathbf{n}_{V2}. \end{aligned} \quad (12)$$

The vector-related Helmholtz free energy density in Eq. (12) disappears in the limit of a homogeneous fluid.

The attractive part of the free energy functional can be expressed as

$$F_{\text{att}} = \frac{1}{2} \sum_{i=1}^K \sum_{j=1}^K \iint \mathbf{dr} \mathbf{dr}' \times \rho_i(\mathbf{r}) \rho_j(\mathbf{r}') g_{ij}(\mathbf{r}, \mathbf{r}') \phi_{ij}^{\text{att}}(|\mathbf{r} - \mathbf{r}'|), \quad (13)$$

where  $K = 1$  for pure fluid and  $K = 2$  for binary mixture. According to the WCA potential model,

$$\phi_{ij}^{\text{att}}(|\mathbf{r} - \mathbf{r}'|) = \begin{cases} -\varepsilon, & |\mathbf{r} - \mathbf{r}'| \leq r_{\min,ij}, \\ 4\varepsilon \left( \frac{\sigma_{ij}^{12}}{|\mathbf{r} - \mathbf{r}'|^{12}} - \frac{\sigma_{ij}^6}{|\mathbf{r} - \mathbf{r}'|^6} \right), & r_{\min,ij} \leq |\mathbf{r} - \mathbf{r}'| \leq r_{\text{cut},ij}, \\ 0, & |\mathbf{r} - \mathbf{r}'| \leq r_{\text{cut},ij}, \end{cases} \quad (14)$$

where  $\sigma_{ij}$  is the soft sphere diameter for pure hydrogen and hydrogen–carbon monoxide mixture.  $r_{\min,ij} = \sqrt[6]{2}\sigma_{ij}$  represents the equilibrium distance between particles.  $r_{\text{cut},ij}$  denotes the cutoff distance. When mean field approximation is used,  $g_{ij}(\mathbf{r}, \mathbf{r}') = 1$ . In WCA perturbation theory, the relation between the hard sphere and soft sphere diameter is obtained by setting the compressibility of hard sphere fluid equal to that of soft sphere reference system, i.e.,

$$\int \mathbf{dr} \{ y^{\text{hs}}(d, r) \exp[-\beta \varepsilon_p^{\text{hs}}(d, r) - 1] \} = \int \mathbf{dr} \{ y^{\text{hs}}(d, r) \exp[-\beta \varepsilon_p^{(0)}(\sigma, r) - 1] \}, \quad (15)$$

where  $\varepsilon_p^{\text{hs}}$  and  $\varepsilon_p^{(0)}$  are, respectively, the pair interaction of hard sphere and the reference system.  $y^{\text{hs}}(d, r) = \exp[\beta \varepsilon_p^{\text{hs}}(d, r)] g^{\text{hs}}(r)$  has identical forms for hard sphere and soft sphere systems. The hard sphere diameter  $d$ , as a function of temperature and density, can be determined from Eq. (15). However, for simplicity of programming, we ignore the temperature and density dependence of hard sphere diameter and assume it to be equal to its soft sphere counterpart. The same assumption has been made by Ball and Evans [38], and Peterson et al. [39].

A spherical Lennard–Jones potential is chosen to represent the interactions between hydrogen and carbon monoxide molecules and carbon atoms. In the Lennard–Jones model, the collision diameter and the energetic well depth are specified as,  $\sigma_{\text{H}_2} = 0.296$  nm and  $\varepsilon_{\text{H}_2}/k = 36.7$  K,  $\sigma_{\text{CO}} = 0.3763$  nm and  $\varepsilon_{\text{CO}}/k = 100.2$  K, and  $\sigma_{\text{C}} = 0.335$  nm and  $\varepsilon_{\text{C}}/k = 28.2$  K, respectively. The cross interaction between the three kinds of particles are calculated by the

Lorentz–Berthelot mixing rules. For simplicity of calculation, the carbon nanotube studied in this work is modeled as a structureless cylindrical pore instead of the real discrete tube wall. This replacement is reasonable because there is little discrepancy between results calculated by the two methods. As described by Stan and Cole [40], the integration of the fluid–solid potential over the cylindrical wall results in the following expression:

$$\psi_{\text{ext}}(r, R) = 3\pi\theta\varepsilon_{\text{fs}}\sigma_{\text{fs}}^2 \left[ \frac{21}{32} \left( \frac{\sigma_{\text{fs}}}{R} \right)^{10} M_{11}(x) - \left( \frac{\sigma_{\text{fs}}}{R} \right)^4 M_5(x) \right], \quad (16)$$

where  $r$  is the distance between the adatom and the nearest point on the cylinder.  $R$  is the radius of the nanotube and  $x = r/R$  is the ratio of distance to radius.  $\theta$  is the surface number density, and has a value of  $38$  nm<sup>-2</sup>.  $\sigma_{\text{fs}}$  is the mixed size parameter of Lennard–Jones potential acted on a fluid molecule and carbon atom. Here the following integrals are used:

$$M_n(x) = \int_0^\pi d\varphi \frac{1}{(1 + x^2 - 2x \cos \varphi)^{n/2}}. \quad (17)$$

As in our previous works [9,21], Simpson integration is applied to calculate the final potential.

Minimization of the grand potential with respect to the density profiles yields the following Euler–Lagrange equation:

$$\rho(r) = \exp \left\{ - \int \mathbf{dr}' \left[ \sum_x \frac{\partial \phi}{\partial n_x} w^{(x)}(r - r') + \rho(r') \phi_{\text{att}}(|r - r'|) \right] + \beta[\mu - \psi_{\text{ext}}(r)] \right\}. \quad (18)$$

### 3. Results and discussions

Picard-type iteration is used to solve Eq. (18) with an initial value of bulk density. To avoid divergence, the old and new densities are mixed in proportion and the iterative process continues until the percentage change of the densities is smaller than  $10^{-6}$ . Trapezoidal integration is used with a step size of  $0.01\sigma_{\text{H}_2}$ , except that some improper integration should be specially treated with the Gauss integration method.

In order to test the validity of the theory, GCMC simulation is also performed to calculate the density distributions of hydrogen and hydrogen–carbon monoxide mixture confined inside an isolated single-walled carbon nanotube. In this calculation, all of the particles are regarded as spheres. Interactions among particles are modeled with Lennard–Jones potential acted on the mass center. As in the DFT calculation, the carbon nanotube wall is treated as a continuous

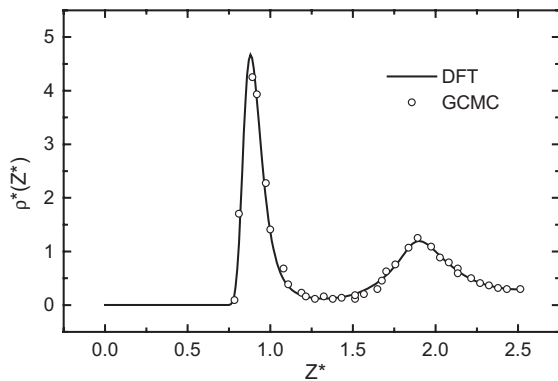
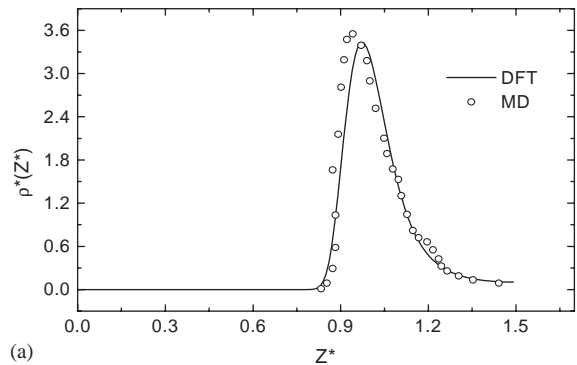


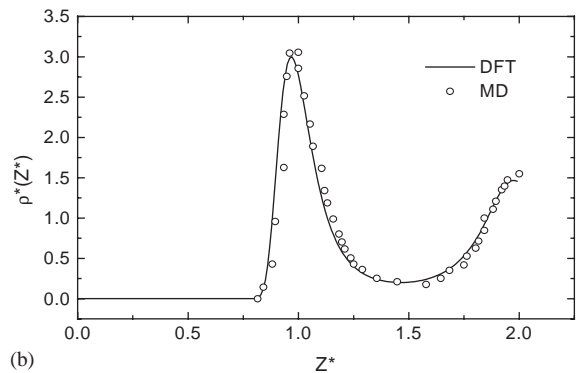
Fig. 1. Density profile for ethylene in a carbon slitlike pore of width  $H^* = 5$  at  $T^* = 1.35$ . The simulation results are from Ref. [43].

surface with certain number density of evenly distributed carbon atoms. To make a fast calculation, the interaction between the fluid and the carbon atom is integrated over the tube surface and regressed to a polynomial. At 300 K and given bulk density, the chemical potential of each component of the fluid is calculated by equation of state and input to the GCMC calculation. The particles are originally placed as an FCC configuration. Three kinds of moves, including displacement, particle creation and particle deletion are performed iteratively with a ratio of 1:1:1, among which, one displacement involves trial moves of all the particles. Due to the equal bulk mole fraction of the binary mixtures, the inserted particles in the tube are chosen with equal ratio from hydrogen and carbon monoxide. Periodic boundary condition is applied only to the axis direction. One million configurations are used to reach equilibrium and another one million to get the system average. At 300 K and bulk density from 0.2 to 0.7 for hydrogen and hydrogen–carbon monoxide, the density profiles inside the tube are calculated and compared with those of DFT calculation.

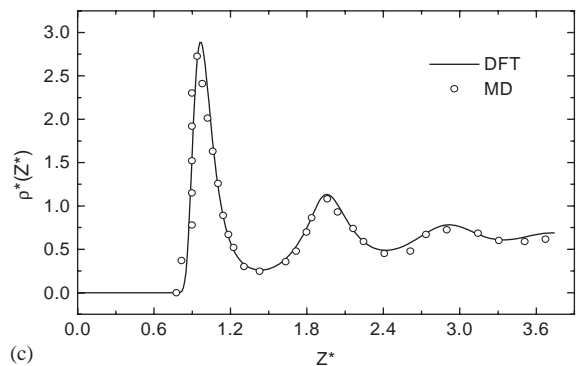
Kierlik and Rosinberg [41] have proposed another version of modified FMT for hard sphere and pure and binary Lennard–Jones fluids [36]. To make comparison, we use the same simulation work as cited in their paper. Among them, the GCMC simulation results of Walton and Quirke [42] and the DFT of this work are plotted in Fig. 1. Fig. 2 shows the comparison between our DFT and the GCMC simulation work of Snook and Van Megen [43]. Their simulation was also confirmed by the molecular dynamics (MD) simulation of Magda et al. [44]. The values of the parameters and the potentials used can be found in the corresponding paper. In these two figures, the results of Kierlik and Rosinberg are not involved, because their results are almost the same as ours, although they used different expressions of the Helmholtz free energy and hard sphere diameter. In their theory, they used four weight functions that are simply related to the successive derivatives of the Heaviside step function and did not use the vector weighted



(a)



(b)



(c)

Fig. 2. Density profiles for a Lennard–Jones fluid in a slitpore at  $T^* = 1.20$  with a width of: (a)  $H^* = 3$ ; (b)  $H^* = 4$ ; (c)  $H^* = 7.5$ . The simulation results are from Refs. [44,45].

density. Moreover, the Helmholtz energy density for hard spheres in their work corresponds to the compressibility equation of the PY theory and the parameters in the expression of hard sphere diameter was obtained by fitting to the liquid densities at coexistence. In spite of these differences, our calculation results agree well with theirs and also with computer simulations data, which confirms the validity of the current method.

In Fig. 3, the density functional calculations of hydrogen adsorption inside single-walled carbon nanotubes are

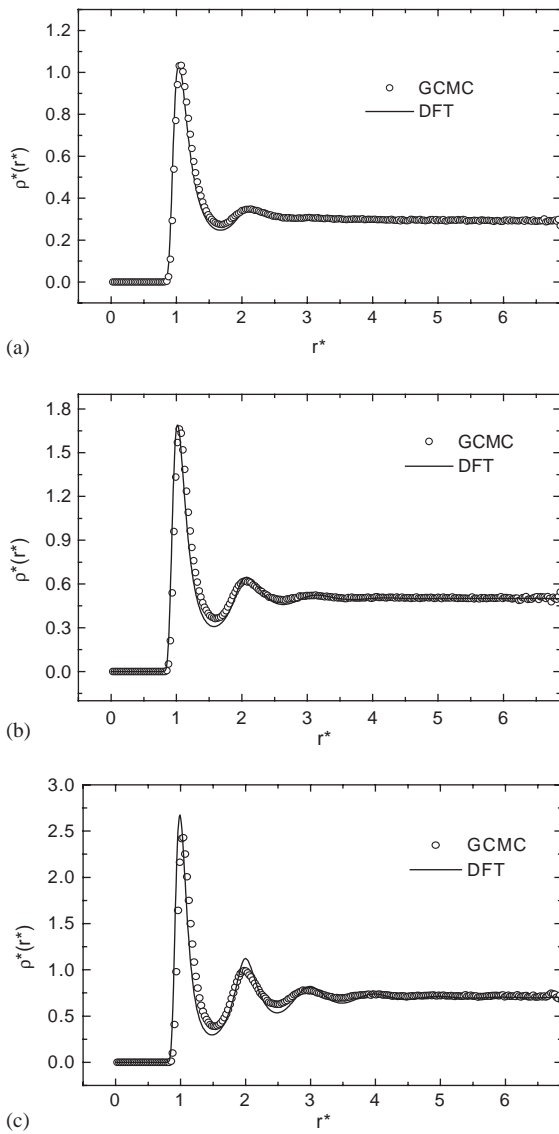


Fig. 3. Density profiles of hydrogen adsorption in single-walled carbon nanotubes at 300 K with the reduced bulk density of: (a) 0.3; (b) 0.5; (c) 0.7.

compared with the GCMC simulation of this work. They have good agreements to each other at low bulk densities, while at high density, for example,  $\rho^* = 0.7$ , the DFT predicts a slightly larger oscillation at the vicinity of the wall. This may due to the selection of hard sphere diameter, which is set to be equal to its soft sphere counterpart.

In Fig. 4(a) and (b), the hydrogen adsorption isotherms inside the carbon nanotubes are calculated via density functional theory. Three sizes of armchair tubes, (18, 18), (30, 30) and (35, 35) are studied. Here, both the total and the excess adsorption are presented. The total adsorption is

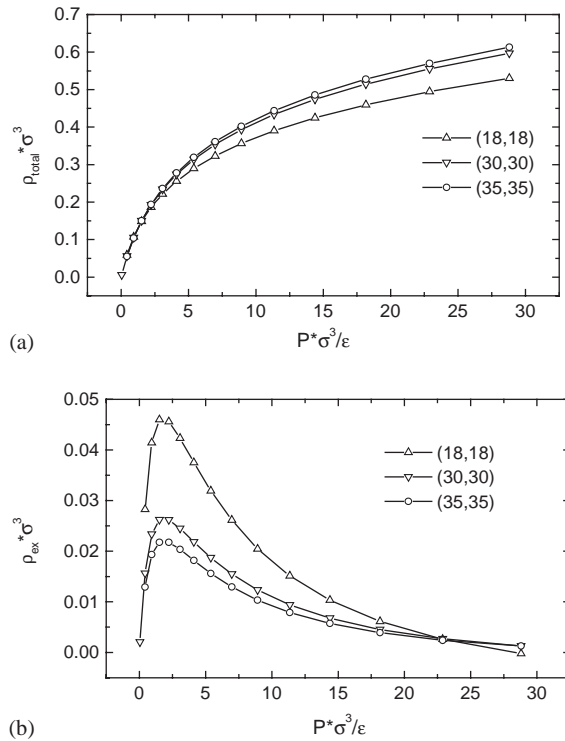


Fig. 4. Predicted adsorption isotherm of hydrogen from DFT at 300 K: (a) the total adsorption; (b) the excess adsorption.

calculated by

$$\Gamma = \frac{2 \int_0^R \rho(r)r dr}{R^2} \tag{19}$$

and the excess adsorption is

$$\Gamma_{ex} = \frac{2 \int_0^R (\rho(r) - \rho_{bulk})r dr}{R^2}, \tag{20}$$

where  $\rho_{bulk}$  is the bulk density and  $R$  is the radius of the tube.

In Fig. 4(a), the total amount of adsorption increases with pressure. At the same temperature, conceptually, the larger tube should hold more particles. But as shown in the figure, this trend is not so evident. This could be explained by Fig. 9(a), in which the particle–tube interactive potential is plotted. Besides space, this interaction is another important factor to affect the amount of adsorption. In Fig. 9(a), the location that has the minimum potential between hydrogen and the wall represents the equilibrium position, and accordingly, the potential value at this position affects the amount of adsorption dramatically. From the figure, one can see that the absolute value of potential has an inverse relation to the tube radius. Therefore, the increase of tube size has a negative contribution to this part of interaction.

The effect of particle–tube interaction becomes more evident when refer to the excess adsorption, which is shown in Fig. 4(b). In the figure, the excess adsorption decreases

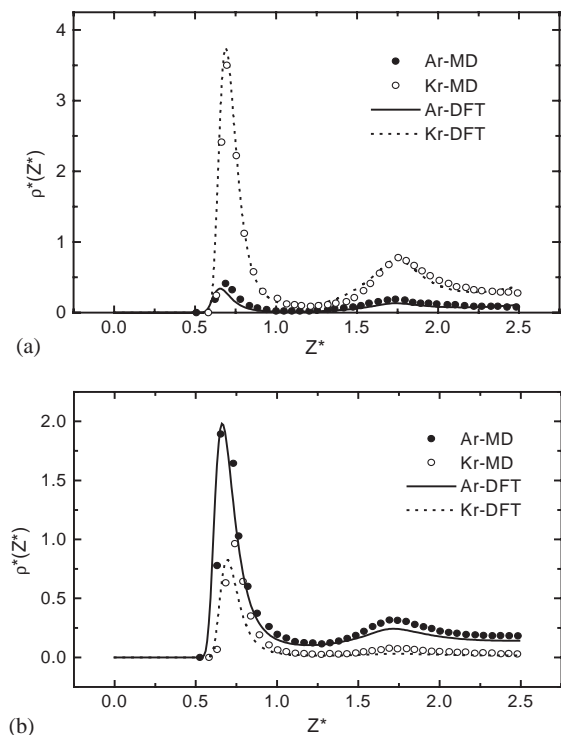


Fig. 5. Density profiles for an argon–krypton mixture adsorbed in a graphite slitlike pore of width  $H^* = 5$  at  $T^* = 2$  (dimensionless quantities are in terms of the argon parameters): (a)  $\rho_b^* = 0.444$ ,  $x_{Ar} = 0.262$ ; (b)  $\rho_b^* = 0.103$ ,  $x_{Ar} = 0.891$ . The simulation results are from Ref. [47].

monotonically with tube size due to the inverse relation between tube radius and the particle–wall interaction. While to each tube,  $\Gamma_{ex}$  has a maximum at reduced pressure of 2.5. This pressure corresponds to the reduced bulk density of about 0.15. After this point, the adsorption decreases with the increase of pressure toward a minimum and then re-increases slightly. The qualitative behavior is similar to that previously found for nitrogen [6] and krypton [45]. As explained by Darkrim [6], there are two competing effects that control the outcome of  $\Gamma_{ex}$ : the repulsive interaction between gas molecules at short distances and the strong attractive interaction between these molecules and the substrate. At low pressures, the attractive interaction dominates, so the higher the pressure, the larger the amount of excess adsorption. While at high pressure, the increase of adsorption with pressure is limited by the effect of repulsive intermolecular interactions, which makes the behavior more like that of hard spheres. However, because only adsorption inside the tube is considered in this work and the interstitial uptake is not included, the effect of which is still not clear. While with an inter-tube separation of 0.315 nm [46], which is far smaller than the tube diameter (a (30,30) tube has a diameter of 4.06 nm), the interstitial region is supposed to give relatively low usable capacity ratios.

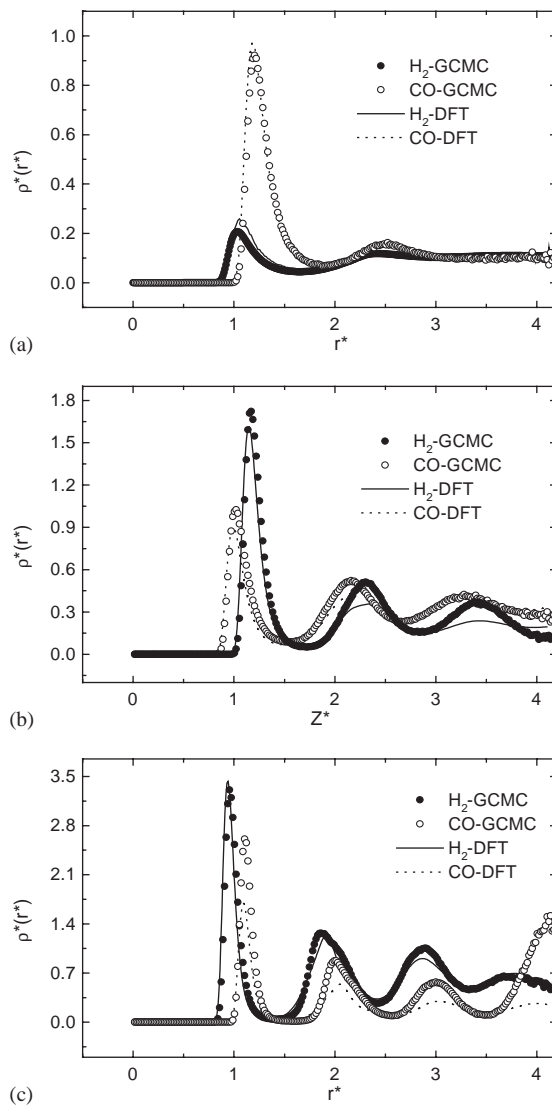


Fig. 6. Density profiles for hydrogen–carbon monoxide mixture adsorbed in (18,18) armchair tube at 300 K with a reduced bulk density of: (a) 0.2; (b) 0.5; (c) 0.7.

Fig. 5 shows the equilibrium density profiles of argon and krypton in a slit pore of width  $H^* = 5$  at  $T^* = 2$ , in which, the MD simulation results of Sokolowski, and Fisher [47] and the DFT calculation of this work are compared. Kierlik and Rosinberg [41] give the results of Fig. 5(a) calculated via their theory, which is not presented in this figure. Results indicate that the density profiles calculated by our model give an agreement with simulation data as good as those in Ref. [41,47], which proves the applicability of this theory to binary mixtures.

Figs. 6 and 7 show the comparison of density profiles of hydrogen and carbon monoxide in (18,18) and (30,30)

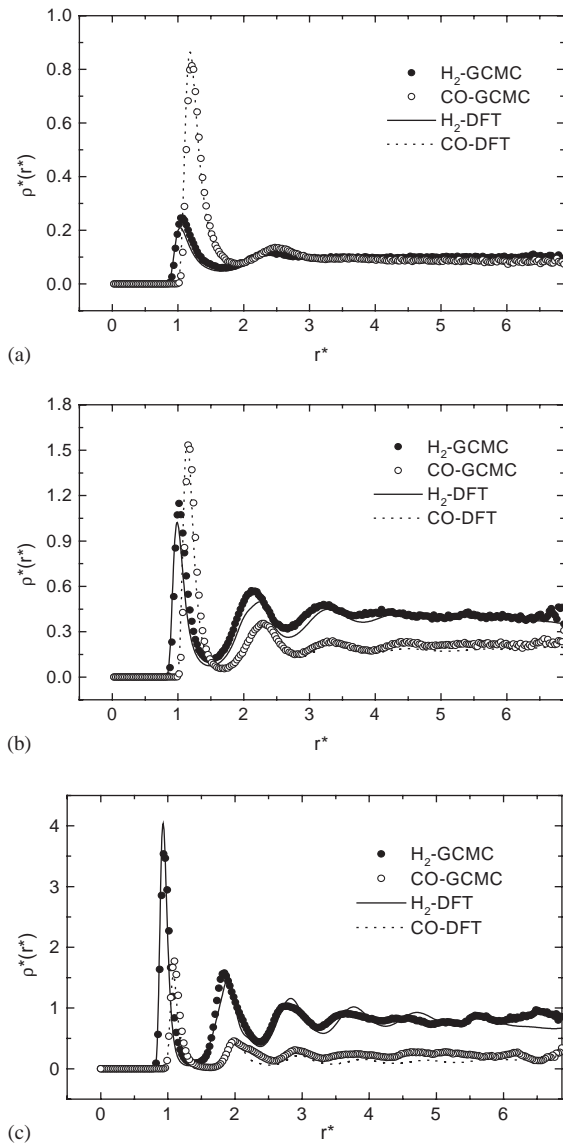


Fig. 7. Same as in Fig. 6, but in a tube of (30,30).

tube calculated by DFT and GCMC in this work. It should be noted that in all of the calculations on binary mixture in this work, the two components have equal mole fraction in the bulk phase. Results show that good agreements are obtained at low density and large tube. However, this functional cannot describe correctly the density profile in small tube, like in Fig. 6(b) and (c). a cylindrical pore with very small diameter can be regarded as a 1D limit of the system, which still remains a difficult challenge for most of 3D density functional [39,41].

The selective adsorption isotherms are plotted in Fig. 8(a). The selectivity is calculated by

$$S = [(1 - x_{H_2}^P)/x_{H_2}^P]/[(1 - x_{H_2}^B)/x_{H_2}^B], \quad (21a)$$

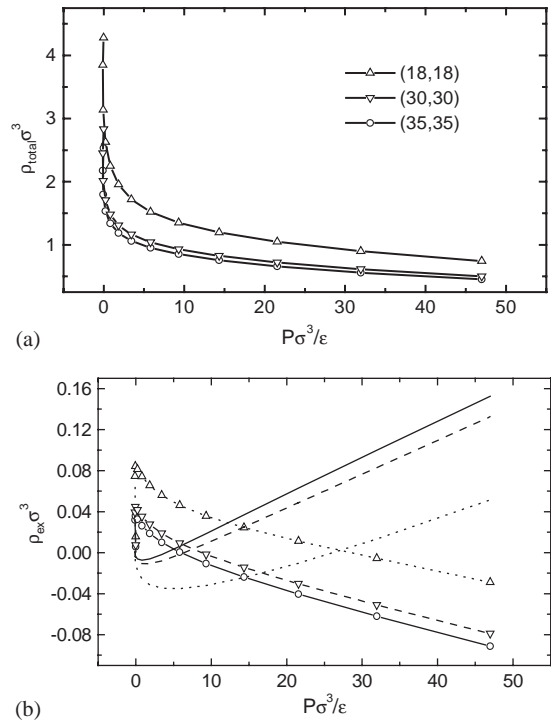


Fig. 8. Predictions from DFT for: (a) selectivity of carbon monoxide at 300 K; (b) excess adsorption of H<sub>2</sub>–CO mixtures; line plus symbols denotes the adsorption of CO, while lines are those of H<sub>2</sub>. Solid lines are for (35,35) tube, dashed lines are for (30,30) tube and dotted lines are for (18,18) tube.

where the upper subscript “P” and “B” denotes pore phase and bulk phase, respectively, and  $x_{H_2} = \rho_{H_2}/(\rho_{H_2} + \rho_{CO})$  is the mole fraction of hydrogen. The following expression can be directly derived from Eq. (21a):

$$S = \frac{\Gamma_{CO}^P/\Gamma_{H_2}^P}{\Gamma_{CO}^B/\Gamma_{H_2}^B}, \quad (21b)$$

where the amount of adsorption  $\Gamma$  is calculated by Eq. (19). It can be concluded from the figure that the selectivity of carbon monoxide in the binary mixture has an inverse relation to both pressure and the tube size. Actually, the competitive adsorption of hydrogen and carbon monoxide is affected by both the energy and the size factors. The energy factor can be qualitatively explained by the difference of the interactive potential between the two kinds of particles and the wall (Fig. 9). As explained in the former paragraph, the minimum potential at the equilibrium position affects dramatically the appearance of the density profile. We have recorded the absolute value of the equilibrium energy difference between the two particles and the wall in the same tube, which are 4.25, 4.45 and 5.04 for (35,35), (30,30) and (18,18), tube, respectively. Evidently, the value increases with the decrease of tube size. It is this value that causes the increase of the selectivity of carbon monoxide at low

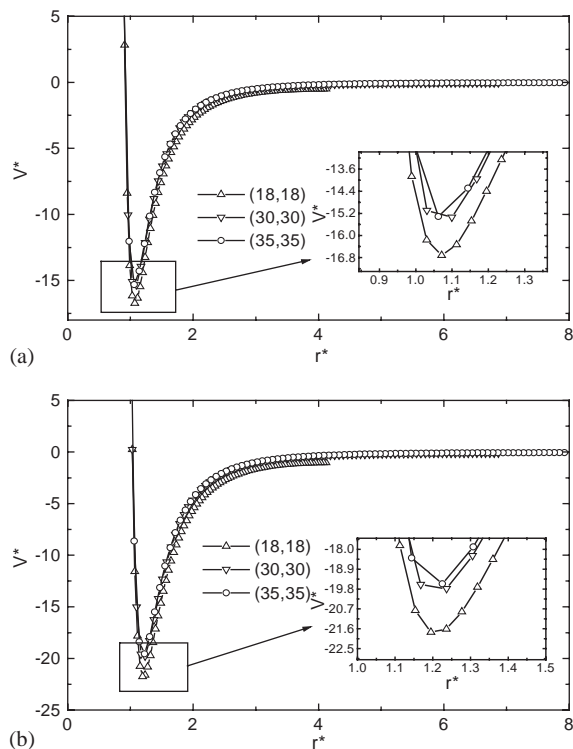


Fig. 9. Particle–wall interactions: (a) H<sub>2</sub>; (b) CO.

pressure. But this is not always the case when the pressure is high. In high-pressure situation, the size factor becomes dominant, which makes the smaller hydrogen molecule more likely to penetrate into the pore than the bigger carbon monoxide molecule. Therefore, with a certain tube size, the selectivity of carbon monoxide decreases with the increase of pressure.

The co-effect of energy and size factor becomes more evident when refers to Fig. 8(b), in which the bulk density is subtracted and the excess density profiles are plotted. In this figure, there are three groups of lines, each contains two branches that cross each other at a certain pressure. The points of intersection indicate the equal mole fractions of the two components and consequently, unit selectivity. The species that is more favorable from the pore changes from carbon monoxide to hydrogen from left to right of the intersection. Moreover, with the increase of tube size, the pressure at the intersection decreases. This is caused by the decrease of the equilibrium energy difference as explained in the preceding paragraph.

#### 4. Conclusions

In this work, a DFT based on the combination of a modified FMT for inhomogeneous hard spheres and the WCA approximation of van de Waals attractions is used to predict the

behavior of pure hydrogen and hydrogen–carbon monoxide mixture at ambient temperature. The density functional is tested by computer simulation results of both this work and other available in literature. Good agreement is achieved for density profiles inside the tube in most of the cases, except for the small-size tube, where the density functional fails to give correct predictions. This reflects the natural inconsistency of most 3D density functionals in 1D limit.

Using the DFT, we calculated the total and excess adsorption isotherms of hydrogen in (18, 18), (30, 30) and (35, 35) armchair nanotubes at 300 K. Results show that the volumetric density of total adsorption increases monotonically with the increase of pressure. While the excess adsorption has a maximum value at reduced pressure of about 2.5. Moreover, within the range of tube size studied in this work, the excess adsorption has an inverse relation to tube radius. This is due to the decrease of particle–wall interaction in larger tubes.

We also calculated the selectivity of carbon monoxide in the binary mixture in (18, 18), (30, 30) and (35, 35) armchair nanotubes at 300 K, which, caused by the co-effect of the energy and size parameters of the two species, has an inverse relation to both pressure and tube size.

In this work, only adsorption inside the tube is calculated, situations in the interstices are not considered. A two-dimensional DFT is going to be applied to the investigation of the adsorption in tube bundles later.

#### Acknowledgements

This work is supported by the National Science and Technology Department through Hydrogen energy 973 project (No. 2000026400) and the Beijing key laboratory of green chemical reaction engineering and technology.

#### References

- [1] Dillon AC, Jones KM, Bekkedahl TA, Kiang CH, Bethune DS, Heben MJ. Storage of hydrogen in single-walled carbon nanotubes. *Nature* 1997;386:377–9.
- [2] Ye Y, Ahn CC, Witham C, Fultz B, Liu J, Rinzler AG, Colbert D, Smith KA, Smalley RE. Hydrogen adsorption and cohesive energy of single-walled carbon nanotubes. *Appl Phys Lett* 1999;74:2307–9.
- [3] Wang QY, Johnson JK. Molecular simulation of hydrogen adsorption in single-walled carbon nanotubes and idealized carbon slit pores. *J Chem Phys* 1999;110:577–86.
- [4] Wang QY, Johnson JK. Hydrogen adsorption on graphite and in carbon slit pores from path integral simulations. *Mol Phys* 1998;95:299–309.
- [5] Wang QY, Johnson JK. Optimization of carbon nanotube arrays for hydrogen adsorption. *J Phys Chem B* 1999;103:4809–13.
- [6] Darkrim F, Vermesse J, Malbrunot P, Levesque D. Monte Carlo simulations of nitrogen and hydrogen physisorption at high pressures and room temperature. Comparison with experiments. *J Chem Phys* 1999;110:4020–7.

- [7] Darkrim F, Levesque D. Monte Carlo simulations of hydrogen adsorption in single-walled carbon nanotubes. *J Chem Phys* 1998;109:4981–4.
- [8] Rzepka M, Lamp P, de la Casa-Lillo MA. Physisorption of hydrogen on microporous carbon and carbon nanotubes. *J Phys Chem B* 1998;102:10894–8.
- [9] Gu C, Gao GH, Yu YX, Mao ZQ. Simulation study of hydrogen storage in single walled carbon nanotubes. *Int J Hydrogen Energy* 2001;26:691–6.
- [10] Gordon PA, Saeger PB. Molecular modeling of adsorptive energy storage: hydrogen storage in single-walled carbon nanotubes. *Ind Eng Chem Res* 1999;38:4647–55.
- [11] Tada K, Furuya S, Watanabe K. Ab initio study of hydrogen adsorption to single-walled carbon nanotubes. *Phys Rev B* 2001;6315:155–405.
- [12] Gelb LD, Gubbins KE. Studies of binary liquid mixtures in cylindrical pores: phase separation, wetting and finite-size effects from Monte Carlo simulations. *Physica A* 1997;244:112–23.
- [13] Cracknell RF, Nicholson D, Quirke N. A grand-canonical Monte-Carlo study of Lennard–Jones mixtures in slit pores 2. Mixtures of 2 center ethane with methane. *Mol Simulation* 1994;13:161–75.
- [14] van de Ven-Lucassen IMJJ, Otten AMVJ, Vlught TJH, Kerkhof PJAM. Molecular dynamics simulation of the Maxwell–Stefan diffusion coefficients in Lennard–Jones liquid mixtures. *Mol Simulation* 1999;23:43–54.
- [15] van de Ven-Lucassen IMJJ, Vlught TJH, van der Zanden AJJ, Kerkhof PJAM. Molecular dynamics simulation of self-diffusion and Maxwell–Stefan diffusion coefficients in liquid mixtures of methanol and water. *Mol Simulation* 1999;23:79–94.
- [16] Gusev VY, O'Brien JA. Prediction of gas mixture adsorption on activated carbon using molecular simulations. *Langmuir* 1998;14:6328–31.
- [17] Samios S, Stubos AK, Kanellopoulos NK, Cracknell RF, Papadopoulos GK, Nicholson D. Determination of micropore size distribution from grand canonical Monte Carlo simulations and experimental CO<sub>2</sub> isotherm data. *Langmuir* 1997;13:2795–802.
- [18] Cracknell RF, Nicholson D. Adsorption of gas mixtures on solid surfaces, theory and computer simulation. *Adsorption J Int Adsorption Soc* 1995;1:7–16.
- [19] Vlught TJH, Krishna R, Smit B. Molecular simulations of adsorption isotherms for linear and branched alkanes and their mixtures in silicalite. *J Phys Chem B* 1999;103:1102–18.
- [20] Bhatia SK. Adsorption of binary hydrocarbon mixtures in carbon slit pores: a density functional theory study. *Langmuir* 1998;14:6231–40.
- [21] Gu C, Gao GH, Yu YX, Nitta T. Simulation for separation of hydrogen and carbon monoxide by adsorption on single-walled carbon nanotubes. *Fluid Phase Equilibria* 2002;194:297–307.
- [22] Sullivan DE. Statistical-mechanics of a nonuniform fluid with long-range attractions. *Phys Rev A* 1982;25:1669–82.
- [23] Tarazona P. Correction. *Phys Rev A* 1985;32:3148.
- [24] Tarazona P. Free-energy density functional for hard-spheres. *Phys Rev A* 1985;31:2672–9.
- [25] Tarazona P, Marconi UMB, Evans R. Phase-equilibria of fluid interfaces and confined fluids—nonlocal versus local density functionals. *Mol Phys* 1987;60:573–95.
- [26] Curtin WA, Ashcroft NW. Weighted-density-functional theory of inhomogeneous liquids and the freezing transition. *Phys Rev A* 1985;32:2909–19.
- [27] Freasier BC, Nordholm S. A generalized vanderwaals model for solvation forces between solute particles in a colloidal suspension. *J Chem Phys* 1983;79:4431–8.
- [28] Rosenfeld Y. Free-energy model for inhomogeneous fluid mixtures—Yukawa-charged hard-spheres, general interactions, and plasmas. *J Chem Phys* 1993;98:8126–48.
- [29] Rosenfeld Y. Phase-separation of asymmetric binary hard-sphere fluids—self-consistent density-functional theory. *Phys Rev Lett* 1994;72:3831–4.
- [30] Rosenfeld Y. Free-energy model for the inhomogeneous hard-sphere fluid mixture and density-functional theory of freezing. *Phys Rev Lett* 1989;63:980–3.
- [31] Rosenfeld Y. Density-functional theory of molecular fluids—free-energy model for the inhomogeneous hard-body fluid. *Phys Rev E* 1994;50:R3318–21.
- [32] Yu YX, Wu J. *J Chem Phys* 2002;117:10156.
- [33] Groh B, Mulder B. Hard-sphere solids near close packing: testing theories for crystallization. *Phys Rev E* 2000;61:3811–22.
- [34] Schmidt M. Fluid structure from density-functional theory. *Phys Rev E* 2000;62:4976–81.
- [35] Roth R, Dietrich S. Binary hard-sphere fluids near a hard wall. *Phys Rev E* 2000;62:6926–36.
- [36] Kierlik E, Rosinberg ML. Density-functional theory for inhomogeneous fluids—adsorption of binary-mixtures. *Phys Rev A* 1991;44:5025–37.
- [37] Rosenfeld Y. Free-energy model for the inhomogeneous hard-sphere fluid—closure relation between generating functionals for direct and cavity distribution-functions. *J Chem Phys* 1990;93:4305–11.
- [38] Ball PC, Evans R. The density profile of a confined fluid—comparison of density functional theory and simulation. *Mol Phys* 1988;63:159–63.
- [39] Peterson BK, Gubbins KE, Heffelfinger GS, Marini U, Marconi B, Vanswol F. Lennard–Jones fluids in cylindrical pores—nonlocal theory and computer-simulation. *J Chem Phys* 1988;88:6487–500.
- [40] Stan G, Cole MW. Low coverage adsorption in cylindrical pores. *Surf Sci* 1998;395:280–91.
- [41] Kierlik E, Rosinberg ML. Free-energy density functional for the inhomogeneous hard-sphere fluid—application to interfacial adsorption. *Phys Rev A* 1990;42:3382–7.
- [42] Walton JPRB, Quirke N. Modeling the phase-behavior of a fluid within a pore. *Chem Phys Lett* 1986;129:382–6.
- [43] Snook IK, Van Megen W. Solvation forces in simple dense fluids 1. *J Chem Phys* 1980;72:2907–13.
- [44] Magda JJ, Tirrell M, Davis HT. Molecular-dynamics of narrow, liquid-filled pores. *J Chem Phys* 1985;83:1888–901.
- [45] Vermesse J, Levesque D. Monte-Carlo simulations of the adsorption of rare-gases at high-pressures. *J Chem Phys* 1994;101:9063–71.
- [46] Saito R, Dresselhaus G, Dresselhaus MS. Physical properties of carbon nanotubes. In: Dresselhaus MS, editors. *Physical properties of carbon nanotubes*. London: World Scientific Publishing Co. Pte. Ltd. 1998. p. 53–7.
- [47] Sokolowski S, Fischer J. Lennard–Jones mixtures in slit-like pores—a comparison of simulation and density-functional theory. *Mol Phys* 1990;71:393–412.